Research Article

Tuning the melting point and phase stability of rare-earth oxides to facilitate their crystal growth from the melt

Matheus PIANASSOLA^{a,b,*}, Kaden L. ANDERSON^{a,b}, Joshua SAFIN^b, Can AGCA^c, Jake W. MCMURRAY^c, Bryan C. CHAKOUMAKOS^d, Jöerg C. NEUEFEIND^d, Charles L. MELCHER^{a,b,e}, Mariya ZHURAVLEVA^{a,b}

^aScintillation Materials Research Center, The University of Tennessee, Knoxville 37996, USA
^bDepartment of Materials Science and Engineering, The University of Tennessee, Knoxville 37996, USA
^cMaterials Science and Technology Division, Oak Ridge National Laboratory, Oak Ridge 37831, USA
^dNeutron Scattering Division, Oak Ridge National Laboratory, Oak Ridge 37831, USA
^eDepartment of Nuclear Engineering, The University of Tennessee, Knoxville 37996, USA

Received: April 30, 2022; Revised: June 13, 2022; Accepted: June 19, 2022 © The Author(s) 2022.

Abstract: The challenge of growing rare-earth (RE) sesquioxide crystals can be overcome by tailoring their structural stability and melting point via composition engineering. This work contributes to the advancement of the field of crystal growth of high-entropy oxides. A compound with only small REs (Lu,Y,Ho,Yb,Er)₂O₃ maintains a cubic C-type structure upon cooling from the melt, as observed via *in-situ* high-temperature neutron diffraction on aerodynamically levitated samples. On the other hand, a compound with a mixture of small and large REs (Lu,Y,Ho,Nd,La)₂O₃ crystallizes as a mixture of a primary C-type phase with an unstable secondary phase. Crystals of compositions (Lu,Y,Ho,Nd,La)₂O₃ and (Lu,Y,Gd,Nd,La)₂O₃ were grown by the micro-pulling-down (mPD) method with a single monoclinic B-type phase, while a powder of (Lu,Y,Ho,Yb,Er)₂O₃ did not melt at the maximum operating temperature of an iridium–rhenium crucible. The minimization of the melting point of the two grown crystals is attributed to the mismatch in cation sizes. The electron probe microanalysis reveals that the general element segregation behavior in the crystals depends on the composition.

Keywords: high-entropy oxides; crystallography; neutron diffraction; crystal growth

1 Introduction

After decades of development and application of crystal growth techniques, the growth of single crystals of rare-earth (RE) oxides via directional solidification is still a challenge. Since the mid-1950s, semiconductors

requirements including (1) a melting point (T_m) compatible with available crucibles and (2) structural stability upon cooling. Compounds that melt above the maximum operating temperature of the widely used iridium crucibles (\sim 2100 °C) [3] are challenging to

and oxides have been grown by pulling single crystals

from the melt via the Czochralski method [1,2]. The success of the growth depends on certain material

grow due to the lack of other practical crucible material.

Additionally, crystals that present phase transitions

* Corresponding author.

E-mail: mpianass@vols.utk.edu

upon cooling have poor structural quality due to the severe cracking that results from the lattice expansion and/or contraction.

RE sesquioxides (RE₂O₃) do not meet those two requirements and because of this, their potential as laser and scintillator crystals has not been fully investigated. All of the RE₂O₃ compounds melt above 2200 °C [4], which surpasses the operating temperature of iridium crucibles. Rhenium crucibles can be used to grow RE₂O₃ crystals, but their high hardness makes crucible fabrication difficult and expensive [5,6]. Upon cooling from the melt, most RE₂O₃ compounds undergo polymorphic transitions and five phases can be observed as a function of temperature and RE ionic radius [7]. Despite not being widely explored in the single-crystal form, RE₂O₃ compounds are attractive as host crystals for high-power lasers due to their low thermal conductivity [8-10], and as high radiation stopping power scintillators due to their high density [11–13]. In both applications, the host RE ion can be easily substituted by an optical activator such as Yb³⁺.

The field of RE₂O₃ crystal growth may benefit from the high-entropy compositional concept as the $T_{\rm m}$ and structural stability can potentially be tuned via composition engineering. An unusual compositional concept introduced by high-entropy alloys [14-16] has recently fostered the development of functional highentropy oxides containing five or more elements in nearly equiatomic amounts [17]. Composition engineering is known to reveal attractive properties in relatively simple compounds [18,19]; the combinatorial possibilities are widely expanded in high-entropy materials, which may allow the tuning of fundamental properties. This inspires an investigation to verify whether the high-entropy compositional design approach can minimize the T_m and suppress polymorphic transitions in RE₂O₃, thus enabling their crystal growth from the melt. To date, reports on the $T_{\rm m}$ and structural stability of high-entropy RE sesquioxides are limited to polycrystalline ceramics, and bulk single crystal growth has not yet been demonstrated [20–23].

In this work, the minimization of the $T_{\rm m}$ and practical aspect of crystal growth of high-entropy RE₂O₃ is demonstrated for the first time. We design three highentropy RE sesquioxides containing Lu, Yb, Er, Y, Ho, Gd, Nd, and La. The RE³⁺ ionic radius (Table 1) was chosen as a formulation criterion to study the effect of cation size mismatch on the $T_{\rm m}$ and phase stability. Composition 1 (Lu,Y,Ho,Yb,Er)₂O₃ contains only small REs, while composition 2 (Lu,Y,Ho,Nd,La)₂O₃ and composition 3 (Lu,Y,Gd,Nd,La)₂O₃ are a mixture of small and large REs. The average ionic radius (AIR) of each composition is listed in Table 2. The structure of the as-prepared samples was evaluated via the powder X-ray diffraction (XRD). Structural stability is evaluated via the in-situ high-temperature neutron diffraction and differential scanning calorimetry (DSC). Crystals were grown from the melt by the micro-pulling-down (mPD) method [24] using an iridium-rhenium 90-10 wt% alloy crucible. The mPD method is ideally suited for this study due to the relatively small amounts of expensive starting materials (~1 g) and faster growth rates that can be achieved compared to scalable techniques such as the Czochralski method [24]. The minimization of the $T_{\rm m}$ in composition 3 is demonstrated via the cooling trace method [25].

2 Methods

2. 1 Composition formulation

To study the effect of the mismatch in cation size in high-entropy RE sesquioxides on melting point, phase formation, and structural stability, eight REs from a wide range of ionic radii were selected. The ionic radius of each trivalent RE cation is listed in Table 1.

Table 1 List of trivalent RE cations and their respective ionic radii for coordination number (CN) VI [26]

RE cation	Lu^{3+}	Yb^{3+}	Er^{3+}	Y^{3+}	Ho^{3+}	Gd^{3+}	Nd^{+}	La^{3+}
Ionic radius for CN VI (Å)	0.848	0.858	0.881	0.892	0.894	0.938	0.995	1.061

Table 2 List of high-entropy RE sesquioxide compositions and their respective AIR for CN VI [26]

Composition number	Chemical formula	AIR for CN VI (Å)	Subjected to neutron diffraction	Grown from the melt
1	(Lu,Y,Ho,Yb,Er) ₂ O ₃	0.875	Yes	No
2	(Lu,Y,Ho,Nd,La) ₂ O ₃	0.938	Yes	Yes
3	(Lu,Y,Gd,Nd,La) ₂ O ₃	0.947	No	Yes

Six REs were selected from the smaller end of that range, Lu, Yb, Er, Y, Ho, and Gd, and two REs from the larger end, Nd and La. Three compositions with equiatomic amounts of REs were formulated, one with only small REs (Lu,Y,Ho,Yb,Er)₂O₃ (commas indicate equiatomic amounts) and two with a mixture of small and large REs, (Lu,Y,Ho,Nd,La)₂O₃ and (Lu,Y,Gd,Nd,La)₂O₃.

2. 2 Steric entrapment synthesis (SES) powder synthesis

Powder samples were synthesized via the polymeric steric entrapment synthesis [27]. Two aqueous solutions were prepared. Solution one had stoichiometric amounts of RE nitrates, RE(NO₃)₃·6H₂O of at least 99.99% purity. Solution two had 80% hydrolyzed polyvinyl alcohol (PVA) of molecular weight of 9000-10,000 g/mol. The amount of PVA was such to produce a positive to negative charge ratio of 4:1; the positive charges come from the RE cations and the negative charges come from the hydroxyl functional group (OH) of PVA. Both solutions were mixed under constant stirring and heated to ~85 °C to evaporate the water, resulting in a precursor foam-type material. This precursor material was dried at ~180 ℃ in air and then calcined at 550 °C for 2.5 h in air. The resulting powder was crystallized at 900 °C for 1 h in air.

2. 3 Bead synthesis

Bead samples were prepared for aerodynamic levitation to allow a containerless sample environment for *in-situ* high-temperature neutron diffraction experiments. The procedure described in this section was performed at the Spallation Neutron Source at Oak Ridge National Laboratory (ORNL). SES powders were melted in a copper hearth using a 400-W continuous-wave CO₂ laser for heating. The samples were rapidly cooled by turning off the laser resulting in 2–3 mm diameter spherical bead samples.

2. 4 Room-temperature XRD

To determine the crystal structure of the as-prepared SES powders and the bead samples, powder XRD patterns were obtained at room temperature using a Panalytical Empyrean diffractometer in the Bragg–Brentano geometry using a Cu Kα X-ray source at 45 kV and 40 mA. Rietveld refinements were performed using General Structure Analysis System II (GSASII) software.

2. 5 In-situ high-temperature neutron diffraction

To evaluate phase transitions upon cooling from the melt and in the temperature range of 1000-2500 °C, the time-of-flight (TOF) neutron diffraction patterns were collected using the Nanoscale-Ordered Materials Diffractometer (NOMAD) at the Spallation Neutron Source at ORNL [28]. An aerodynamic levitator, a 400-W continuous-wave CO₂ laser, and a singlewavelength (0.9 µm) optical pyrometer (Chino Inc.) were used to provide a containerless environment and enable data collection at elevated temperatures [29–31]. Two compositions were selected for neutron diffraction experiments, composition 1 (Lu,Y,Ho,Yb,Er)₂O₃ and composition 2 (Lu,Y,Ho,Nd,La)₂O₃. Bead samples were levitated using high-purity Ar gas in an Ar-filled chamber. The sample temperature was varied by adjusting the CO₂ laser power. The empty conical nozzle levitator and a Si bead were measured at room temperature for normalization and correction of all patterns.

Initially, the samples were melted on the levitator, and then the laser power was slowly decreased to solidify the sample. 5-min scans were performed to determine whether the sample was molten or crystallized. After finding the solidification point, 2-h scans were performed at constant temperatures in the range of 1000–2500 °C with a cooling rate of ~20 °C/min between scans. The standard deviation of the temperature measurements was smaller than 30 °C for all scans. Powder-like diffraction patterns were collected by ensuring the random rotation of the bead samples, which was achieved by controlling the Ar gas flow through the aerodynamic nozzle levitator. The best signal-to-noise ratio was observed for the 65° scattering bank of the NOMAD instrument, which was used for structure refinement. Rietveld refinement was performed using GSASII software in the range of 3.3-18.4 ms TOF.

2.6 DSC

To identify any phase transitions in the 30–1300 °C temperature range, the DSC curves were obtained for the as-prepared bead samples. The samples were ground in a mortar and placed in alumina crucibles. A Labsys EVO instrument was used to obtain the DSC curves with a heating and cooling rate of 5 °C/min.

2. 7 Crystal growth

Crystals were grown using the mPD method, which is

optimal for material development due to the small amount of material necessary (~1 g) to evaluate the growability of novel compounds. A KDN mPD furnace (Dai-Ichi Kiden, Japan) equipped with a radio frequency (RF) generator model TR-02001 operated at 26 kVA was used. The mPD growth method and setup were previously described in detail [32]. A 16-mm diameter iridium-rhenium alloy crucible (20 wt% Re) with a 3-mm diameter die and a 0.5-mm diameter capillary channel was used to grow cylindrical crystals. The as-prepared powder samples were placed in the crucible, which was heated inductively to melt the samples. An iridium pin was used as a seed to initiate the growth. The crucible temperature cannot be assessed during growth since the crucible is held within alumina insulation tubes. However, the RF power used during all growth experiments is the same as the one used to previously grow Lu₂SiO₅ crystals from the same crucible in the same growth setup. Therefore, the maximum crucible temperature in this work is estimated to be slightly above 2150 °C, which is the melting point of Lu₂SiO₅.

2. 8 Electron probe microanalysis

A 1-mm thick cross-section sample was cut from the seed end and tail end of the crystals. The samples were embedded in epoxy and then polished for the elemental composition analysis. Concentration profiles were obtained by using a CAMECA SX100 Electron Microprobe operated at a voltage of 15 kV and a current of 30 nA. Images were acquired by high-speed backscattered electron detectors. Compositional information was obtained by detecting characteristic X-rays with wavelength-dispersive spectrometers. Radial concentration profiles were obtained by collecting data in 100- μ m steps. The probe point size was 1 μ m, and the excitation area diameter was in the 2–3 μ m range.

2. 9 Melting point measurements

The cooling trace method was used for the determination of liquidus temperatures in the (Lu,Y,Gd,Nd,La)₂O₃ system and consists in melting samples and recording their temperature upon cooling. A temperature peak during cooling indicates the recalescence phenomenon, and the peak maximum is assigned as the sample liquidus temperature [25]. The optical pyrometers are commonly used to measure such high temperature, and the spectral emissivity of the sample should be known

for accurate measurements. The spectral emissivity of multi-RE samples was calculated as a weighted average of the spectral emissivities of the single-RE sesquioxides formed by the constituent REs. The following experiments were performed at the Spallation Neutron Source at ORNL. To obtain the spectral emissivity of the constituent sesquioxides, powders of Lu₂O₃, Y₂O₃, Gd₂O₃, Nd₂O₃, and La₂O₃ of at least 99.99% purity were individually melted in a copper hearth to form 2-3 mm diameter spherical beads; a 400-W continuouswave CO₂ laser was used for heating. The bead samples were placed on an aerodynamic levitator and levitated using a 80% Ar-20% O₂ gas mixture to obtain a containerless sample environment and avoid any possible reactions with crucible material. The samples were then heated using the CO2 laser and melted under levitation. Their spectral emissivity was determined using their reported melting temperatures in Refs. [33–36].

To determine the effect of the number of REs on the liquidus temperature in the compositional (Lu, Y, Gd, Nd, La)₂O₃ system, three compounds, (Lu,Y,Gd)₂O₃, (Lu,Y, Gd,Nd)₂O₃, and (Lu,Y,Gd,Nd,La)₂O₃, were prepared via the steric entrapment. As described for the single-RE powders, the three multi-RE samples were prepared as 2-3 mm diameter beads and placed on an aerodynamic levitator. The samples were then heated using the CO₂ laser and melted under levitation. After a 5-s dwell at the molten state, the heating laser was shut off. The temperature profile was recorded using a singlewavelength (0.9 µm) optical pyrometer (Chino Inc.) with a data acquisition rate of 25 Hz and an operating temperature range of 600-3000 °C. The temperature was corrected by Wien's law [37]. This procedure was repeated at least six times for each sample.

3 Results and discussion

3. 1 Structure of as-prepared samples

Synthesis temperature and AIR are known to affect phase formation in high-entropy RE sesquioxides [21,38], and therefore samples of compositions 1, 2, and 3 were prepared with two distinct thermal histories for structural evaluation. Samples referred to as "SES powders" were made via the SES [27], crystallized at 900 $^{\circ}$ C, and cooled slowly. Samples referred to as "beads" are 2–3 mm diameter spheres made by melting SES powders in a copper hearth with a CO₂ laser as a

heat source; the beads were rapidly cooled from the melt by turning off the laser. Phase formation in these samples may follow the polymorphic behavior of single-RE sesquioxides. As seen in Fig. 1, five polymorphs are formed as a function of temperature and ionic radius of single-RE sesquioxides [7]. This diagram of polymorphic transformations will be used to correlate synthesis temperature, AIR, and phase formation of SES powders and bead samples.

Although Fig. 1 has been traditionally adopted to study RE₂O₃ [7,39,40], a few considerations should be

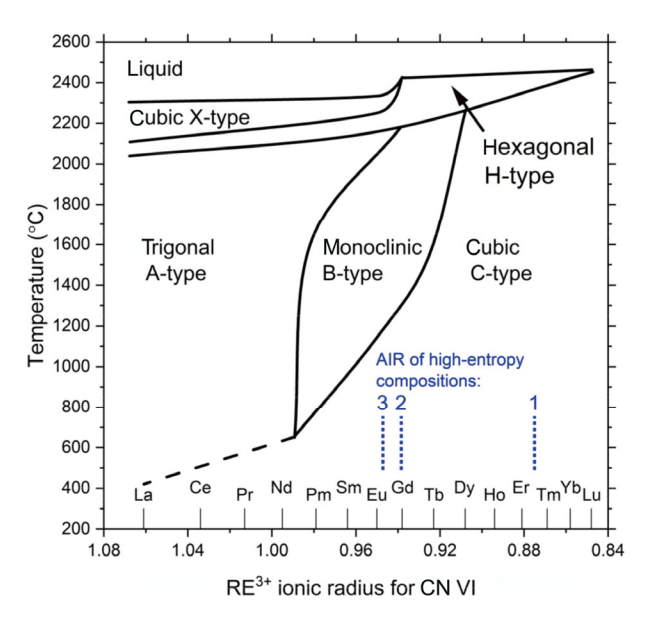


Fig. 1 Schematic diagram of polymorphic transformations for single-RE RE₂O₃ as a function of temperature and RE ionic radius for CN VI [7,26]. The relative horizontal position of the AIR of the high-entropy compositions 1 (Lu,Y,Ho,Yb,Er)₂O₃, 2 (Lu,Y,Ho,Nd,La)₂O₃, and 3 (Lu,Y,Gd,Nd,La)₂O₃ are indicated as the vertical dashed lines.

mentioned. First, some data points used to construct the diagram are controversial. For instance, a few authors report on Yb₂O₃ with the H-type structure [4], while some publications indicate that Yb₂O₃ maintains the C-type structure until its melting [41,42]. Second, an additional phase is formed when two REs with a difference in ionic radii of at least 0.20 Å are mixed in equal amounts. Compounds such as LaLuO₃ have an orthorhombic perovskite structure (space group *Pnma*) [43–45] and are not predicted in Fig. 1 since they are not single-RE RE₂O₃.

A single cubic C-type phase (space group $Ia\overline{3}$) was identified for SES powders of compositions 1, 2, and 3, as indicated by the powder XRD patterns in Fig. 2(a). In fact, the C-type phase could be predicted in Fig. 1. The AIR of compositions 1, 2, and 3 (indicated in Fig. 1) lie in the C-type region at the synthesis temperature of SES powders, 900 °C. Both compositions 2 and 3 have large La³⁺ and Nd³⁺ ions that do not form the C-type structure in La₂O₃ and Nd₂O₃. This may lead to a lattice distortion, which would explain the higher degree of crystallinity seen as sharper XRD reflection peaks of the SES powders of composition 1 compared to compositions 2 and 3 (Fig. 2(a)).

In the bead samples, composition 1 is also a single C-type phase, while both compositions 2 and 3 have a single monoclinic B-type phase (space group C2/m), as seen in Fig. 2(b). The beads are expected to retain high-temperature structures at room temperature since they were rapidly cooled from the melt. Therefore, composition 1 may not undergo phase transitions in a large range of temperatures since both the SES powders and the bead of composition 1 are a single C-type phase. On the other hand, compositions 2 and 3

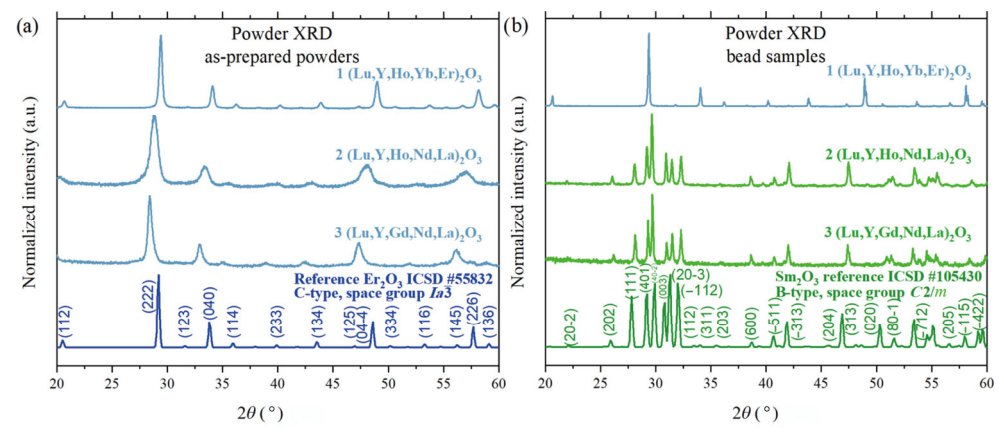


Fig. 2 Room-temperature powder XRD patterns: (a) As-prepared powders have a single C-type phase; a reference reflection pattern of Er_2O_3 is shown for comparison. (b) Bead sample of composition 1 maintains the single C-type phase, while the beads of compositions 2 and 3 are a single B-type phase; a reference pattern of Sm_2O_3 is shown for comparison.

undergo a phase transformation from the low-temperature C-type phase to the high-temperature B-type phase. This C- to B-type phase transition follows the trend of polymorphic behavior in single-RE sesquioxides, as observed by the relative position of the AIR of compositions 2 and 3 in Fig. 1.

Composition 1 is a promising candidate for crystal growth since the single C-type structure is observed after slow cooling from 900 °C and after fast cooling from the melt. Compositions 2 and 3 may also be promising, as they could potentially retain a B-type structure when cooled slowly from the melt after crystal growth. To further evaluate the structural stability of the high-entropy RE sesquioxide compounds proposed here, high-temperature structural characterization is necessary.

3. 2 High-temperature structural stability upon cooling from the melt

To evaluate the structural stability upon cooling from the melt, beads of compositions 1 (Lu,Y,Ho,Yb,Er)₂O₃ and 2 (Lu,Y,Ho,Nd,La)₂O₃ were subjected to *in-situ* high-temperature neutron diffraction using the NOMAD

instrument at ORNL. Composition 3 (Lu,Y,Gd,Nd,La)₂O₃ is not included here because Gd has a large neutron absorption cross-section [46] which makes the data quality poor. A containerless sample environment was achieved by using a conical nozzle levitator in an Ar atmosphere and a CO₂ laser for heating. This unique experimental setup allowed extremely temperatures (~2500 °C) to be achieved without the need of refractory sample holders. To investigate the structure of the beads, a room-temperature pattern was initially acquired. The beads were then melted at 2550–2600 °C; the molten state was confirmed by collecting a diffraction pattern and ensuring the absence of reflection peaks. The beads were then cooled slowly (20 °C/min) to obtain diffraction patterns at fixed temperatures in the range of 1000–2500 $^{\circ}$ C.

The bead of composition 1 (Lu,Y,Ho,Yb,Er)₂O₃ is a single C-type phase at room temperature (before heating) and in the 1000–2500 $^{\circ}$ C temperature range. The room-temperature C-type structure agrees with the powder XRD results in Fig. 2(b). Diffraction patterns obtained at 2456 \pm 16, 1640 \pm 19, and 1114 \pm 17 $^{\circ}$ C are seen in Fig. 3(a); a single C-type phase was confirmed

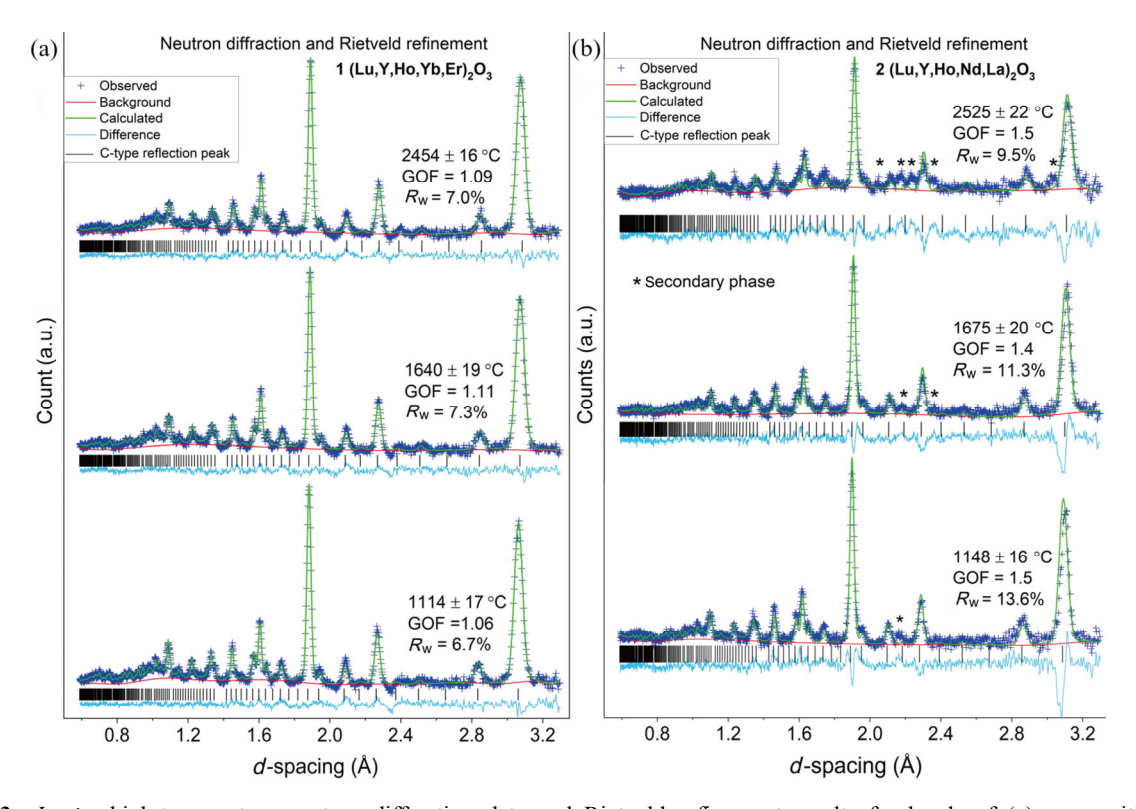


Fig. 3 *In-situ* high-temperature neutron diffraction data and Rietveld refinement results for beads of (a) composition 1 (Lu,Y,Ho,Yb,Er)₂O₃ and (b) composition 2 (Lu,Y,Ho,Nd,La)₂O₃. Sample temperature is indicated in each pattern. The bead of composition 1 is a single C-type phase, and the bead of composition 2 is a mixture of a primary C-type phase with an unknown secondary phase. Goodness-of-fit (GOF) values are included in Fig. 3.

via Rietveld refinement. The stability of the C-type structure upon cooling from the melt makes composition 1 a promising candidate for the growth of high-quality crystals. A combination of REs of similar, small ionic radii in composition 1 may have constrained the lattice into a single C-type phase over a wide temperature range [22]. Therefore, selecting REs of similar ionic radii may be essential to suppress polymorphic transformations in high-entropy RE sesquioxides.

The structure of the bead of composition 2 (Lu,Y, Ho,Nd,La)₂O₃ could not be determined at room temperature by neutron diffraction due to the low signal-to-noise ratio of the data. The pattern obtained at room temperature before heating resembles the expected one for the monoclinic structure identified via the XRD in Fig. 2(b). However, Rietveld structure refinement using neutron diffraction data was inconclusive due to a low signal-to-noise ratio. To better use the beam-time, high-temperature measurements were prioritized.

A mixture of a primary C-type phase with an unknown secondary phase was observed for a bead of composition 2 in the ~1000-2500 °C temperature range. Patterns collected at 2525 \pm 22, 1675 \pm 20, and 1148 ± 16 °C are shown in Fig. 3(b). During Rietveld refinement, the secondary phase peaks indicated in Fig. 3(b) could not be matched with any of the expected phases in Fig. 1 or with the orthorhombic perovskite structure typical of LaLuO₃. This may suggest a suboxide structure. This bead sample lost ~2/3 of its mass during the measurements due to evaporation; and this is likely due to the fact that Nd₂O₃ and La₂O₃ have the highest vapor pressures among all single-RE sesquioxides [47]. The resulting composition fluctuation may explain the variation in number and intensity of the secondary peaks with decreasing the temperature, as seen in Fig. 3(b).

For a composition that tends to evaporate at temperatures close to their $T_{\rm m}$, the mass loss is expected to be pronounced for the bead samples due to their large specific surface area. The relative mass loss is expected to be less pronounced for melt reservoirs used in crystal growth due to the larger volume of material. Therefore, composition 2 is not discarded for crystal growth experiments, since the effects of evaporation on phase composition may be distinct from those observed for the bead samples during the high-temperature neutron diffraction experiments.

In general, the refined lattice parameter of the C-

type structure in the bead of composition 1 is smaller than that of composition 2, as seen in Fig. 4. This is expected since the AIR of composition 1 (0.875 Å) is smaller than that of composition 2 (0.938 Å). Additionally, the lattice parameter of composition 1 increases linearly with temperature ($R^2 = 0.99$), while the lattice parameter of the bead of composition 2 also increases with temperature, but with a significant deviation from linearity ($R^2 = 0.95$). This may result from both composition fluctuation in the bead of composition 2 due to sample evaporation and a possible cation exchange between the C-type phase and the secondary phase [37].

3. 3 Evaluation of phase stability in the range of 30–1300 ℃

To identify possible low-temperature phase transitions in the as-prepared bead samples, the DSC curves were obtained in Fig. 5. The initial structure of the beads was C-type for composition 1 and B-type for compositions 2 and 3 (Fig. 2(b)). No endothermic or exothermic peaks were identified in the DSC curves, which indicates that none of the bead samples undergo phase transitions in the 30–1300 °C temperature range. Therefore, all the three compositions are attractive for crystal growth experiments.

3.4 Crystal growth

Crystals of compositions 2 (Lu,Y,Ho,Nd,La)₂O₃ and

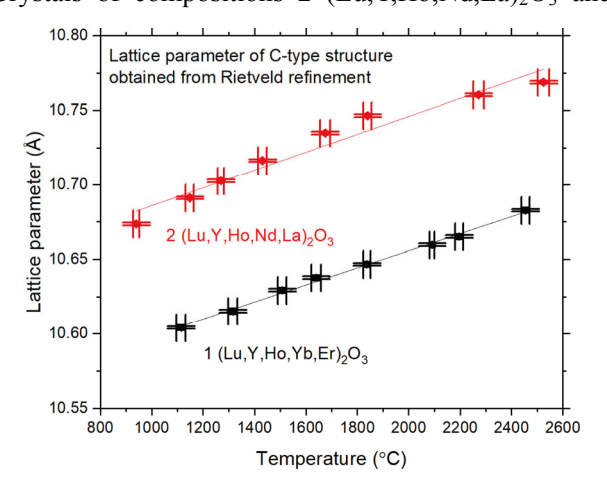


Fig. 4 Lattice parameters of the C-type structure were obtained via Rietveld structure refinement from neutron diffraction data collected for beads of compositions 1 and 2. In general, the bead of composition 2 (AIR = 0.938 Å) has larger lattice parameters than those of composition 1 (AIR = 0.875 Å) due to its larger AIR. Linear regression fits are shown for each dataset.

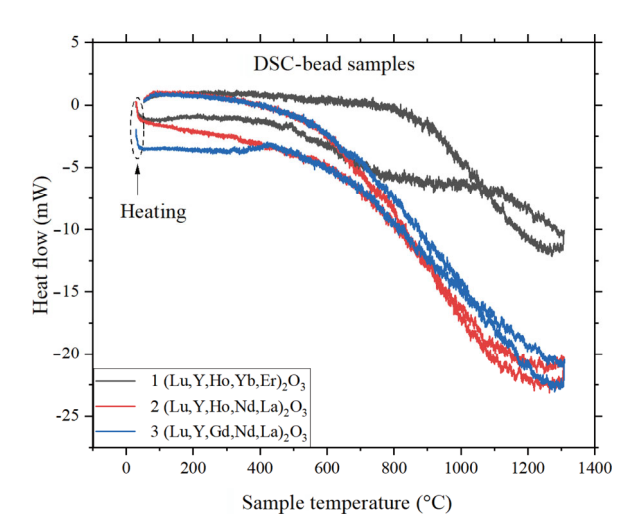


Fig. 5 DSC curves were measured on the as-prepared bead samples in air. The temperature range is 30-1300 °C, and the heating and cooling rate is 5 °C/min.

3 (Lu,Y,Gd,Nd,La)₂O₃ were grown by the mPD method using an iridium–rhenium 90–10 wt% alloy crucible, which demonstrates the practical aspect of growing high-entropy RE sesquioxides crystals with a $T_{\rm m}$ minimized via composition engineering. Hereafter these crystals are referred to as "crystal 2" and "crystal 3". The powder of composition 1 (Lu,Y,Ho,Yb,Er)₂O₃ did not melt at the crucible's maximum operating temperature. This indicates that compositions 2 and 3 have lower $T_{\rm m}$ than 1 and the mixture of small and large REs in compositions 2 and 3 may favor the minimization of the $T_{\rm m}$.

Figure 6(a) shows the top view of the crucible with the sintered SES powders of composition 1 after the growth attempt. Figures 6(b) and 6(c) show the grown crystals 2 and 3, respectively. The seed end and tail end of the crystals are indicated in Fig. 6 and correspond to the first and last portion to be solidified, respectively. Intense sample evaporation was observed during the growth of crystals 2 and 3, which may compromise the composition homogeneity of the crystal. The powder XRD data of the samples after the growth experiments are similar to those of the bead samples in Fig. 2(b) and indicate a single C-type phase for the sintered SES powders of composition 1 and a single B-type phase for both crystals 2 and 3.

3. 5 Melting temperatures in the (Lu,Y,Gd,Nd,La)₂O₃ system

We hypothesize that the larger number of REs in a sesquioxide, the lower the $T_{\rm m}$. The $T_{\rm m}$ can be described as the ratio between the enthalpy of fusion $\Delta H_{\rm fus}$ and



Fig. 6 (a) Top view of the iridium–rhenium crucible with sintered powder of composition 1 that did not melt at the maximum operating temperature of the crucible. (b) Crystal of composition 2. (c) Crystal of composition 3.

the entropy of fusion ΔS_{fus} , thus $T_{\text{m}} = \Delta H_{\text{fus}} / \Delta S_{\text{fus}}$. By increasing the number of REs in a compound, the $\Delta S_{\rm fus}$ is expected to increase, minimizing the $T_{\rm m}$. To verify that, the T_m of the multi-RE sesquioxides $(Lu, Y, Gd)_2O_3$, $(Lu, Y, Gd, Nd)_2O_3$, and $(Lu, Y, Gd, Nd, La)_2O_3$ were measured via the cooling trace method [25]. The measured $T_{\rm m}$ of the multi-RE samples are significantly lower than those of single-RE sesquioxides formed by the constituent REs as seen in Fig. 7. Additionally, as the nominal number of REs increases, the $T_{\rm m}$ decreases, which results from an increasing ΔS_{fus} . The sample of composition 3 (Lu,Y,Gd,Nd,La)₂O₃ melts below 2200 °C, which allowed the crystal growth of this compound as discussed in Section 3.4. This minimization of $T_{\rm m}$ with an increasing number of REs may be composition-dependent since a (La,Sm,Dy,Er, Nd)₂O₃ sample has been reported with a higher melting point than its constituent oxides [23]. This unexpected increase in $T_{\rm m}$ was attributed to a nonideal mixing in the solid and/or the liquid phases, and therefore the effects of complex compositions and local ordering on the $T_{\rm m}$ need to be further investigated.

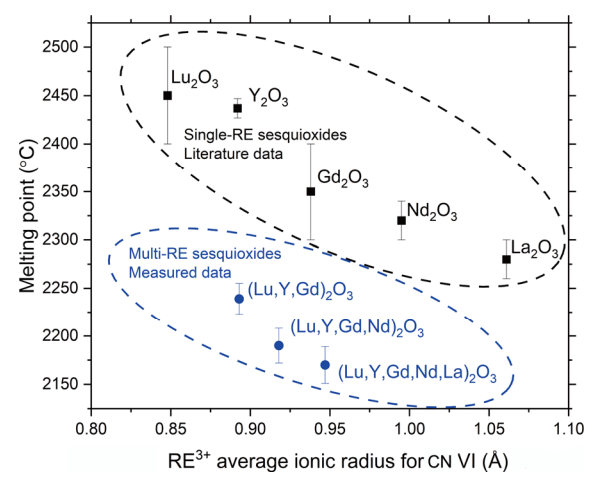


Fig. 7 Measured melting points of the compositions from the system of composition 3 (Lu,Y,Gd,Nd,La)₂O₃ (blue circles) are lower than those of Lu₂O₃ [33], Y₂O₃ [36], Gd₂O₃ [35], Nd₂O₃ [33], and La₂O₃ [36] (black squares).

3. 6 Elemental distribution profiles in the grown crystals

To evaluate the elemental distributions in the crystals, radial concentration profiles were obtained via the electron probe microanalysis (EPMA) on thin disks cut from the grown crystals and are shown in Fig. 8. On the tail end of crystal 2 (Lu,Y,Ho,Nd,La)₂O₃ (Fig. 8, left), the concentration data are more continuous than those of the seed end (Fig. 8, right) because the melt flow at the solidification front may not have been completely equilibrated at the beginning of the growth. The fact that the relative concentration of Lu is higher than that of the other elements may be related to the composition fluctuation resulting from the significant sample evaporation during growth.

The elemental segregation in the mPD crystals is evaluated by the shape of the radial concentration

profile. Flat profiles indicate a segregation coefficient $k \approx 1$, downwardly curved profiles indicate k < 1 (which results from the rejection of the element by the growing crystal), and upwardly curved profiles indicate k > 1 (which results from the preferential incorporation) [24,32]. In Fig. 8, Lu and Nd have close-to-flat profiles and do not segregate significantly; Y and Ho have upwardly curved profiles and are preferentially incorporated; and La has a downwardly curved profile and is rejected.

Although compositions 2 (Lu,Y,Ho,Nd,La)₂O₃ and 3 (Lu,Y,Gd,Nd,La)₂O₃ are similar, Lu is rejected by crystal 3 but not by crystal 2. The EPMA concentration profiles of crystal 3 are shown in Fig. 9, in which Lu has downwardly curved profiles. Similar to crystal 2, Nd has a flat profile in crystal 3, Y and Gd (which substitutes Ho in crystal 2) have upwardly curved

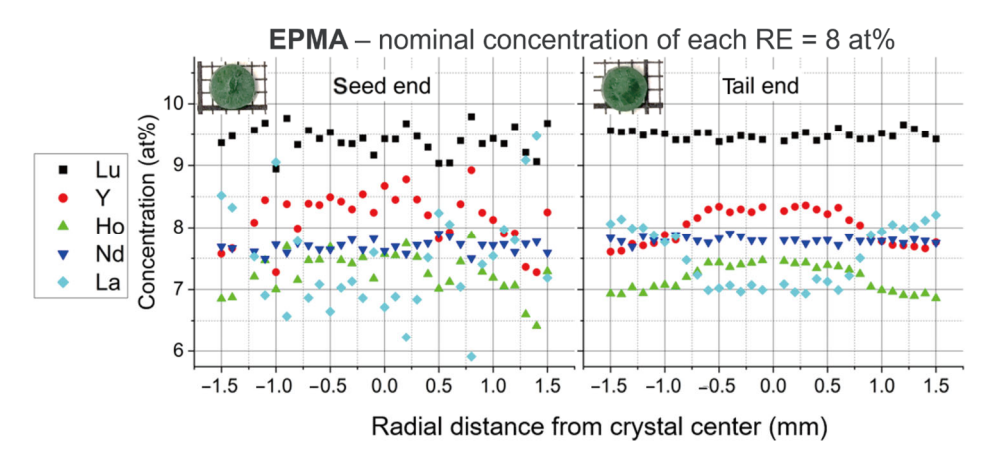


Fig. 8 EPMA radial concentration profiles of seed end (left) and tail end (right) of crystal 2. The legend on the left applies to both graphs. On the vertical axis, −1.5 and 1.5 mm correspond to the last measurement toward the outer surface of the crystal; zero corresponds to the center of the crystal.

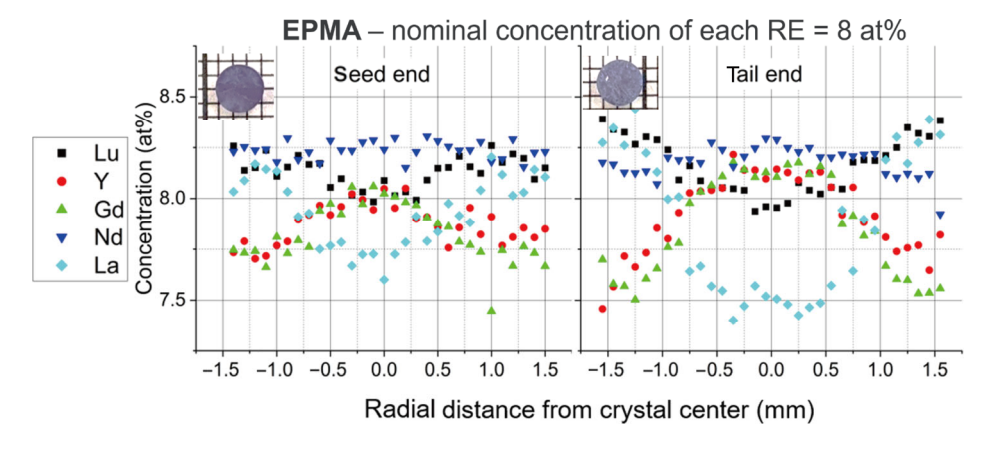


Fig. 9 EPMA radial concentration profiles of seed end (left) and tail end (right) of crystal 3. The legend on the left applies to both graphs. On the vertical axis, -1.5 and 1.5 mm correspond to the last measurement toward the outer surface of the crystal; zero corresponds to the center of the crystal.

profiles, and La has a downwardly curved profile. The lower La concentration on the tail end of crystal 3 may indicate the gradual evaporation of La, such that the melt was depleted in La toward the end of the growth. Further studies on growth parameters such as pulling rate may result in crystals with a more homogeneous elemental distribution [32]. Additionally, adding a small percentage of oxygen in the growth atmosphere may prevent sample evaporation and favor composition homogeneity [48].

4 Conclusions

Composition engineering is the key to designing structurally stable high-entropy RE sesquioxides. Mixing only small REs in composition 1 (Lu,Y,Ho,Yb,Er)₂O₃ led to a stable C-type phase, which was formed upon crystallization of melt and was preserved upon cooling. Therefore, cations with similar ionic radii may favor the structural stability of these sesquioxides. Mixing small and large REs in composition 2 (Lu,Y,Ho,Nd,La)₂O₃ led to the formation of a primary C-type phase with an unstable secondary phase upon cooling from the melt. Therefore, cations with a wide range of ionic radii may hinder the structural stability of high-entropy RE sesquioxides.

Structural analysis at temperatures around the melting point of high-entropy RE sesquioxides was possible due to a unique containerless sample environment achieved via aerodynamic levitation of bead samples. This experimental setup was essential to acquire the *in-situ* high-temperature neutron diffraction patterns using the NOMAD instrument at ORNL.

Melting points of high-entropy RE sesquioxides are affected by the composition. While the powder of composition 1 did not melt at the maximum operating temperature of an iridium–rhenium crucible, those of compositions 2 and 3 (Lu,Y,Ho,Nd,La)₂O₃ did melt and could be grown by the mPD method. This indicates that compounds with a significant mismatch in cation sizes such as compositions 2 and 3 may melt at lower temperatures than compounds with a more limited range of cation sizes such as composition 1.

Further investigation into growth parameters such as pulling rate and growth atmosphere may lead to highentropy RE sesquioxide crystals with better optical quality and composition homogeneity. Additionally, doping these crystals with optically active REs such as Ce³⁺, Pr³⁺, and Yb³⁺ may reveal attractive luminescent properties for scintillation and laser applications.

Acknowledgements

This work was supported by the National Science Foundation (DMR 1846935). The authors are grateful for the support from the Center for Materials Processing, The University of Tennessee. The powder XRD was performed at the Institute for Advanced Materials & Manufacturing Diffraction Facility, The University of Tennessee, Knoxville. The electron microprobe measurements were performed at the Electron Microprobe Laboratory in the Department of Earth and Planetary Sciences, The University of Tennessee, Knoxville, with the assistance of Molly MCCANTA and Allan PATCHEN. A portion of this research used resources at the Spallation Neutron Source, a DOE Office of Science User Facility operated by the Oak Ridge National Laboratory.

References

- [1] Uecker R. The historical development of the Czochralski method. *J Cryst Growth* 2014, **401**: 7–24.
- [2] Brandle CD. Czochralski growth of oxides. J Cryst Growth 2004, 264: 593–604.
- [3] Yoshikawa A, Nikl M, Boulon G, *et al.* Challenge and study for developing of novel single crystalline optical materials using micro-pulling-down method. *Opt Mater* 2007, **30**: 6–10.
- [4] Zhang YM, Jung IH. Critical evaluation of thermodynamic properties of rare earth sesquioxides (RE = La, Ce, Pr, Nd, Pm, Sm, Eu, Gd, Tb, Dy, Ho, Er, Tm, Yb, Lu, Sc and Y). *Calphad* 2017, **58**: 169–203.
- [5] Fukabori A, Chani V, Kamada K, et al. Growth of Y₂O₃, Sc₂O₃ and Lu₂O₃ crystals by the micro-pulling-down method and their optical and scintillation characteristics. J Cryst Growth 2011, 318: 823–827.
- [6] Fukabori A, Chani V, Kamada K, et al. Growth of Yb-doped Y₂O₃, Sc₂O₃, and Lu₂O₃ single crystals by the micro-pulling-down technique and their optical and scintillation characterization. J Cryst Growth 2012, 352: 124–128.
- [7] Adachi Gy GY, Imanaka N. The binary rare earth oxides. Chem Rev 1998, 98: 1479–1514.
- [8] Beil K, Saraceno CJ, Schriber C, et al. Yb-doped mixed sesquioxides for ultrashort pulse generation in the thin disk laser setup. Appl Phys B 2013, 113: 13–18.
- [9] Kränkel C. Rare-earth-doped sesquioxides for diodepumped high-power lasers in the 1-, 2-, and 3-μm spectral range. *IEEE J Sel Top Quantum Electron* 2015, 21: 250– 262.

- [10] Kränkel C, Uvarova A, Haurat É, *et al*. Czochralski growth of mixed cubic sesquioxide crystals in the ternary system Lu₂O₃–Sc₂O₃–Y₂O₃. *Acta Crystallogr Sect B* 2021, 77: 550–558.
- [11] Rétot H, Blahuta S, Bessière A, et al. Improved scintillation time response in (Lu_{0.5}Gd_{0.5})₂O₃:Eu³⁺compared with Lu₂O₃: Eu³⁺transparent ceramics. J Phys D Appl Phys 2011, 44: 235101.
- [12] Futami Y, Yanagida T, Fujimoto Y, *et al.* Optical and scintillation properties of Sc₂O₃, Y₂O₃ and Lu₂O₃ transparent ceramics synthesized by SPS method. *Radiat Meas* 2013, **55**: 136–140.
- [13] Yanagida T, Fujimoto Y, Yagi H, et al. Optical and scintillation properties of transparent ceramic Yb:Lu₂O₃ with different Yb concentrations. Opt Mater 2014, 36: 1044–1048.
- [14] Cantor B, Chang ITH, Knight P, et al. Microstructural development in equiatomic multicomponent alloys. *Mater Sci Eng A* 2004, 375–377: 213–218.
- [15] Yeh JW, Chen SK, Lin SJ, et al. Nanostructured highentropy alloys with multiple principal elements: Novel alloy design concepts and outcomes. Adv Eng Mater 2004, 6: 299–303.
- [16] Miracle DB, Senkov ON. A critical review of high entropy alloys and related concepts. *Acta Mater* 2017, 122: 448–511.
- [17] Rost CM, Sachet E, Borman T, *et al.* Entropy-stabilized oxides. *Nat Commun* 2015, **6**: 8485.
- [18] Trukhanov AV, Kostishyn VG, Panina LV, *et al.* Control of electromagnetic properties in substituted M-type hexagonal ferrites. *J Alloys Compd* 2018, **754**: 247–256.
- [19] Trukhanov AV, Turchenko VO, Bobrikov IA, *et al*. Crystal structure and magnetic properties of the BaFe_{12-x}Al_xO₁₉ (x = 0.1-1.2) solid solutions. *J Magn Magn Mater* 2015, **393**: 253–259.
- [20] Djenadic R, Sarkar A, Clemens O, *et al.* Multicomponent equiatomic rare earth oxides. *Mater Res Lett* 2017, **5**: 102–109.
- [21] Pianassola M, Loveday M, McMurray JW, *et al.* Solid-state synthesis of multicomponent equiatomic rare-earth oxides. *J Am Ceram Soc* 2020, **103**: 2908–2918.
- [22] Tseng KP, Yang Q, McCormack SJ, *et al.* High-entropy, phase-constrained, lanthanide sesquioxide. *J Am Ceram Soc* 2020, **103**: 569–576.
- [23] Ushakov SV, Hayun S, Gong WP, et al. Thermal analysis of high entropy rare earth oxides. Materials 2020, 13: 3141.
- [24] Fukuda T, Chani VI. *Shaped Crystals: Growth by the Micro-Pulling-Down Technique*. Berlin, Germany: Springer Berlin Heidelberg, 2007.
- [25] Agca C, Neuefeind JC, McMurray JW, et al. Melting temperature measurement of refractory oxide ceramics as a function of oxygen fugacity using containerless methods. J Am Ceram Soc 2020, 103: 4867–4875.
- [26] Shannon RD, Prewitt CT. Effective ionic radii in oxides and fluorides. *Acta Crystallogr Sect B Struct Sci Cryst Eng Mater* 1969, **25**: 925–946.

- [27] Nguyen MH, Lee SJ, Kriven WM. Synthesis of oxide powders by way of a polymeric steric entrapment precursor route. *J Mater Res* 1999, **14**: 3417–3426.
- [28] Neuefeind J, Feygenson M, Carruth J, et al. The nanoscale ordered materials diffractometer NOMAD at the spallation neutron source SNS. Nucl Instrum Methods Phys Res Sect B Beam Interact Mater Atoms 2012, 287: 68–75.
- [29] Calder S, An K, Boehler R, et al. A suite-level review of the neutron powder diffraction instruments at Oak Ridge National Laboratory. Rev Sci Instrum 2018, 89: 092701.
- [30] Skinner LB, Benmore CJ, Weber JKR, et al. Structure of molten CaSiO₃: Neutron diffraction isotope substitution with aerodynamic levitation and molecular dynamics study. J Phys Chem B 2012, 116: 13439–13447.
- [31] Benmore CJ, Weber JKR. Aerodynamic levitation, supercooled liquids and glass formation. *Adv Phys X* 2017, **2**: 717–736.
- [32] Pianassola M, Loveday M, Chakoumakos BC, *et al.* Crystal growth and elemental homogeneity of the multicomponent rare-earth garnet (Lu_{1/6}Y_{1/6}Ho_{1/6}Dy_{1/6}Tb_{1/6}Gd_{1/6})₃Al₅O₁₂. *Cryst Growth Des* 2020, **20**: 6769–6776.
- [33] Glushko VP, Thermicheskie KV. Thermal Constants of Substances. Moscow: VINITI, 1981.
- [34] Ackermann RJ, Rauh EG. The thermodynamic properties of substoichiometric yttrium sesquioxide. *J Chem Thermodyn* 1973, **5**: 331–340.
- [35] Curtis CE, Johnson JR. Ceramic properties of samarium oxide and gadolinium oxide; X-ray studies of other rareearth oxides and some compounds. *J Am Ceram Soc* 1957, **40**: 15–19.
- [36] Foex M, Traverse JP. Investigations about crystalline transformation in rare earths sesquioxides at high temperatures. *Rev Int Hautes Temp Refract* 1966, **3**: 429–453. (in French)
- [37] Wien W. XXX. On the division of energy in the emission-spectrum of a black body. *The London, Edinburgh, and Dublin Philosophical Magazine and Journal of Science* 1897, **43**: 214–220.
- [38] Tseng KP, Yang Q, McCormack SJ, et al. High-entropy, phase-constrained, lanthanide sesquioxide. *J Am Ceram Soc* 2020, **103**: 569–576.
- [39] Zinkevich M. Thermodynamics of rare earth sesquioxides. *Prog Mater Sci* 2007, **52**: 597–647.
- [40] Fedorov PP, Nazarkin MV, Zakalyukin RM. On polymorphism and morphotropism of rare earth sesquioxides. *Crystallogr Rep* 2002, **47**: 281–286.
- [41] Badie JM. Phases et transitions de phases à haute température dans les systèmes Sc₂O₃–Ln₂O₃ (Ln = lanthanide et yttrium). *Rev Int Hautes Temp Refract* 1978, **15**: 183–199. (in French)
- [42] Pavlik A, Ushakov SV, Navrotsky A, *et al*. Structure and thermal expansion of Lu₂O₃ and Yb₂O₃ up to the melting points. *J Nucl Mater* 2017, **495**: 385–391.
- [43] Ovanesyan KL, Petrosyan AG, Shirinyan GO, *et al.* Single crystal growth and characterization of LaLuO₃. *Opt Mater* 1998, **10**: 291–295.

- [44] Uecker R, Bertram R, Brützam M, et al. Large-lattice-parameter perovskite single-crystal substrates. *J Cryst Growth* 2017, **457**: 137–142.
- [45] Ito K, Tezuka K, Hinatsu Y. Preparation, magnetic susceptibility, and specific heat on interlanthanide perovskites ABO₃ (A = La–Nd, B = Dy–Lu). *J Solid State Chem* 2001, **157**: 173–179.
- [46] Sears VF. Neutron scattering lengths and cross sections. *Neutron News* 1992, **3**: 26–37.
- [47] Jacobson NS. Thermodynamic Properties of Some Metal Oxide-Zirconia Systems. Cleveland, USA: National Aeronautics and Space Administration Lewis Research Center, 1989.
- [48] Tomm Y, Reiche P, Klimm D, et al. Czochralski grown Ga₂O₃ crystals. J Cryst Growth 2000, 220: 510–514.

Open Access This article is licensed under a Creative Commons Attribution 4.0 International License, which permits use, sharing, adaptation, distribution and reproduction in any medium or format, as long as you give appropriate credit to the original author(s) and the source, provide a link to the Creative Commons licence, and indicate if changes were made.

The images or other third party material in this article are included in the article's Creative Commons licence, unless indicated otherwise in a credit line to the material. If material is not included in the article's Creative Commons licence and your intended use is not permitted by statutory regulation or exceeds the permitted use, you will need to obtain permission directly from the copyright holder.

To view a copy of this licence, visit http://creativecommons.org/licenses/by/4.0/.